A simple functional form for proton-nucleus total reaction cross sections

K. Amos* and P. K. Deb†

School of Physics, The University of Melbourne, Victoria, 3010, Australia

(Dated: January 28, 2003)

Abstract

A simple functional form has been found that gives a good representation of the total reaction cross sections for the scattering of protons from (15) nuclei spanning the mass range ^{9}Be to ^{238}U and for proton energies ranging from 20 to 300 MeV.

*Electronic address: amos@physics.unimelb.edu.au
†Electronic address: deb@physics.unimelb.edu.au

I. INTRODUCTION

Total reaction cross sections of nucleon scattering from nuclei (stable as well as radioactive) are the most basic nuclear observables [1] being the sum of all the reaction processes induced during nuclear collisions. Reliable methods of predicting these values accurately and quickly are needed for a variety of applications [2]; applications which include the production of radioactive ion beams [3], studies of the relative abundances of the nuclei in galactic cosmic rays [4], as well as for radiation shielding design for future space exploration vehicles [5]. Some others of quite current interest concern the transmutation of long lived radioactive waste into shorter lived products using accelerator driven systems (ADS) [6, 7, 8] and in predicting dosimetry for patients in radiation therapy [9]. To be able to specify those total reaction cross sections in a simple functional form then has great utility for any associated evaluation such as of nucleon production in spallation calculations.

Recently [10] nucleon-nucleus total reaction cross sections to 300 MeV for ^{12}C and ^{208}Pb have been predicted in good agreement with data. Cross sections were evaluated using g-folding optical potentials formed by full folding realistic two nucleon (NN) interactions with credible nucleon-based structure models of those nuclei. In particular, the ground state of ^{12}C was specified from a complete $(0+2)\hbar\omega$ shell model evaluation [10], while that of ^{208}Pb was obtained from a Skyrme-Hartree-Fock calculation [11]. The effective interactions at each energy in the range to 300 MeV were defined from the NN g matrices (solutions of the Bruckner-Bethe-Goldstone equations) of the free NN (BonnB) interactions. Consequently they vary with energy and the medium density. The resulting nA optical potentials are complex, energy dependent and non-local. All details of the approach and numerous demonstrations of its successful use with targets spanning the entire mass range (3 to 238) are given in the recent review [12]. But each such prediction of nucleon scattering is an involved calculation that culminates with use of large scale computer programs, and those of DWBA98 [12, 13] in recent studies.

It would be very utilitarian if aspects of such scattering were indeed well approximated by a simple convenient functional form. We demonstrate herein that for the total reaction cross sections such a form may exist for nuclei spanning the mass range. In all we report results from 15 nuclei ranging in mass from 9 to 238. Also we have studied proton scattering for energies ranging from 20 MeV to 300 MeV.

II. A SIMPLE FUNCTIONAL FORM FOR $p-A$ TOTAL REACTION CROSS SECTIONS

Initially we have used a set of g-folding optical potential calculations to specify proton-nucleus scattering S matrices, i.e with energies $E \propto k^2$,

$$S_l^{\pm} \equiv S_l^{\pm}(k) = e^{2i\delta_l^{\pm}(k)} = \eta_l^{\pm}(k) e^{2i\Re\left[\delta_l^{\pm}(k)\right]} \ , \tag{1}$$

where $\delta_l^{\pm}(k)$ are the (complex) scattering phase shifts and $\eta_l^{\pm}(k)$ are the moduli of the S matrices. The superscript designates $j = l \pm 1/2$. Therefrom total reaction cross sections

are predicted by

$$\begin{aligned}\sigma_R(E) &= \frac{\pi}{k^2}\sum_{l=0}^{\infty}\left\{(l+1)\left[1-\left(\eta_l^+\right)^2\right]+l\left[1-\left(\eta_l^-\right)^2\right]\right\} \\ &= \frac{\pi}{k^2}\sum_{l=0}^{\infty}\sigma_l^{(R)}(E)\ . \end{aligned} \tag{2}$$

The partial reaction cross sections $\sigma_l^{(R)}(E)$ so found we now take as 'data', and such will be so specified hereafter. We note that there are discrepancies between the predictions of total reaction cross sections found using the g-folding approach and actual data due to limitations in that approach, e.g. in the structure model used to describe the ground state densities of some nuclei. However there have been so many successes with the approach [10, 12, 14] that we believe the functional form developed here on the basis of g-folding potential calculated values is pertinent with but minor refinement (of the values of the three parameter values) to reproduce actual measured total reaction cross sections.

As will be evident from the figures presented later, the results clearly suggest that such partial reaction cross sections can be described by a simple functional form such as

$$\sigma_l^{(R)}(E) = (2l+1)\left[1+e^{\frac{(l-l_0)}{a}}\right]^{-1} + \epsilon(2l_0+1)e^{\frac{(l-l_0)}{a}}\left[1+e^{\frac{(l-l_0)}{a}}\right]^{-2}\ , \tag{3}$$

in which the parameters, $l_0(E,A)$, $a(E,A)$, and $\epsilon(E,A)$, should vary smoothly with energy and mass.

The summation giving the total reaction cross section can be limited to a value l_{max} and the associated form tends appropriately to the known high energy limit. With increasing energy, l_{max} becomes so large that the exponential fall of the functional form, Eq. 3, can be approximated as a straight vertical line ($l_0 = l_{max}$). In that case, the total reaction cross section equates to the area of a triangle and

$$\sigma_R \Rightarrow \frac{\pi}{2k^2}l_{max}(2l_{max}+1) \approx \frac{\pi}{k^2}l_{max}^2\ . \tag{4}$$

Then with $l_{max} \sim kR$, at high energies, $\sigma_R \Rightarrow \pi R^2$; the geometric cross section as required.

For any dynamical situation in which numerous partial reaction cross sections contribute non-negligibly to the sum in Eq. 2, one can use the limit form

$$\sigma_R(E) = \frac{\pi}{k^2}\sum_{l=0}^{\infty}\sigma_l^{(R)}(E) \Longrightarrow \frac{\pi}{k^2}\int_0^{\infty}\sigma^{(R)}(E;\lambda)\ d\lambda\ . \tag{5}$$

Then with $x = \frac{\lambda - l_0}{a}$ and using the basic integrals

$$\begin{aligned}\int_{-l_0/a}^{\infty}\frac{1}{1+e^x}dx &= \left[\int_0^{l_0/a}\frac{1}{1+e^{-x}}dx + \int_0^{\infty}\frac{e^{-x}}{1+e^{-x}}dx\right] \\ &= \frac{l_0}{a} + \sum_{n=1}^{\infty}(-)^{n+1}e^{-\frac{l_0}{a}n} \\ \int_{-l_0/a}^{\infty}\frac{x}{1+e^x}dx &= \left[-\int_0^{l_0/a}\frac{x}{1+e^{-x}}dx + \int_0^{\infty}\frac{xe^{-x}}{1+e^{-x}}dx\right] \\ &= -\frac{1}{2}\frac{l_0^2}{a^2} + 1.645 + \sum_{n=1}^{\infty}(-)^n\left(1+\frac{1}{n^2}\right)e^{-\frac{l_0}{a}}\ , \end{aligned} \tag{6}$$

the integral observable is

$$\begin{aligned}
\sigma^{(R)}(E) &= \frac{\pi}{k^2}\sum_l \sigma_l^{(R)}(E) \rightarrow \frac{\pi}{k^2}\int_0^\infty \sigma^{(R)}(E;\lambda)\, d\lambda \\
&= \frac{\pi}{k^2}\Bigg\{ l_0(l_0+1) + 3.29a^2 + a\epsilon(2l_0+1) \\
&\quad + \sum_{n=0}^{\infty} e^{-n\frac{l_0}{a}}(-)^n \left[2a^2\left\{1+\frac{1}{n^2}\right\} + (2l_0+1)\left\{a\epsilon - \frac{1}{n}\right\}\right]\Bigg\} \\
&\underset{n=1}{\rightarrow} \frac{\pi}{k^2}\Bigg\{ l_0(l_0+1) + 3.29a^2 + a\epsilon(2l_0+1) \\
&\qquad + \left[(2l_0+1)\{1-a\epsilon\} - 4a^2\right] e^{-\frac{l_0}{a}}\Bigg\} \qquad (7)
\end{aligned}$$

We have used this (n=1) integral form for all energies and masses and, as could be expected, results are not good when the number of significant partial wave terms is small, as is the case for low energies. But from those comparisons, limit conditions for application of the integral representation are evident.

III. RESULTS

We have calculated the partial reaction cross sections, σ_l(E), of the scattering of protons from 15 different nuclei, namely ^{9}Be, ^{12}C, ^{16}O, ^{19}F, ^{27}Al, ^{40}Ca, ^{63}Cu, ^{90}Zr, ^{118}Sn, ^{140}Ce, ^{159}Tb, ^{181}Ta, ^{197}Au, ^{208}Pb and ^{238}U. The results from the calculations using the g-folding optical potentials (the data) were then fit using the simple functional form given in Eq. 3. The comparisons are displayed in Figs. 1 through 5. In these figures, the solid lines represent the results calculated using the simple functional form. The dots are the data. We have considered protons with 10 different energies for each nucleus and the partial reaction cross sections for each nucleus are shown in the figures by different symbols according to the proton energy. Specifically we use the symbol shown after each number for energies of 20 [empty circles], 30 [filled circles], 40 [empty squares], 50 [filled squares], 65 [empty diamonds], 100 [filled diamonds], 150 [empty up triangles], 200 [filled up triangles], 250 [empty down triangles] and 300 [filled down triangles] MeV. For each mass there is a clear progression in the data with energy; one that is similar over the entire mass range studied and, in fact, was the motivation for our search for an analytic function to describe all of that data.

At low energies, 20 MeV especially and for the light masses most evidently, there are few significant partial wave contributions to the reaction cross sections. The peak of these partial wave reaction cross section data thus is not large and occurs at small values of l. Concomitantly, the 3 parameter fit function will involve small values of l_0 and the fit to the (limited) data set may not be as uniquely determined as at higher energies, particularly as the associated variations of σ_l (data and calculated result) are not dominated by the straight line factor $(2l+1)$ at low l-values. Also the individual data values, for 20 MeV and light mass targets, are more sensitive to details of the actual optical potentials used than is the case for the corresponding problem of matching the σ_l values at higher energies (and target mass) with the 3 parameter functional form.

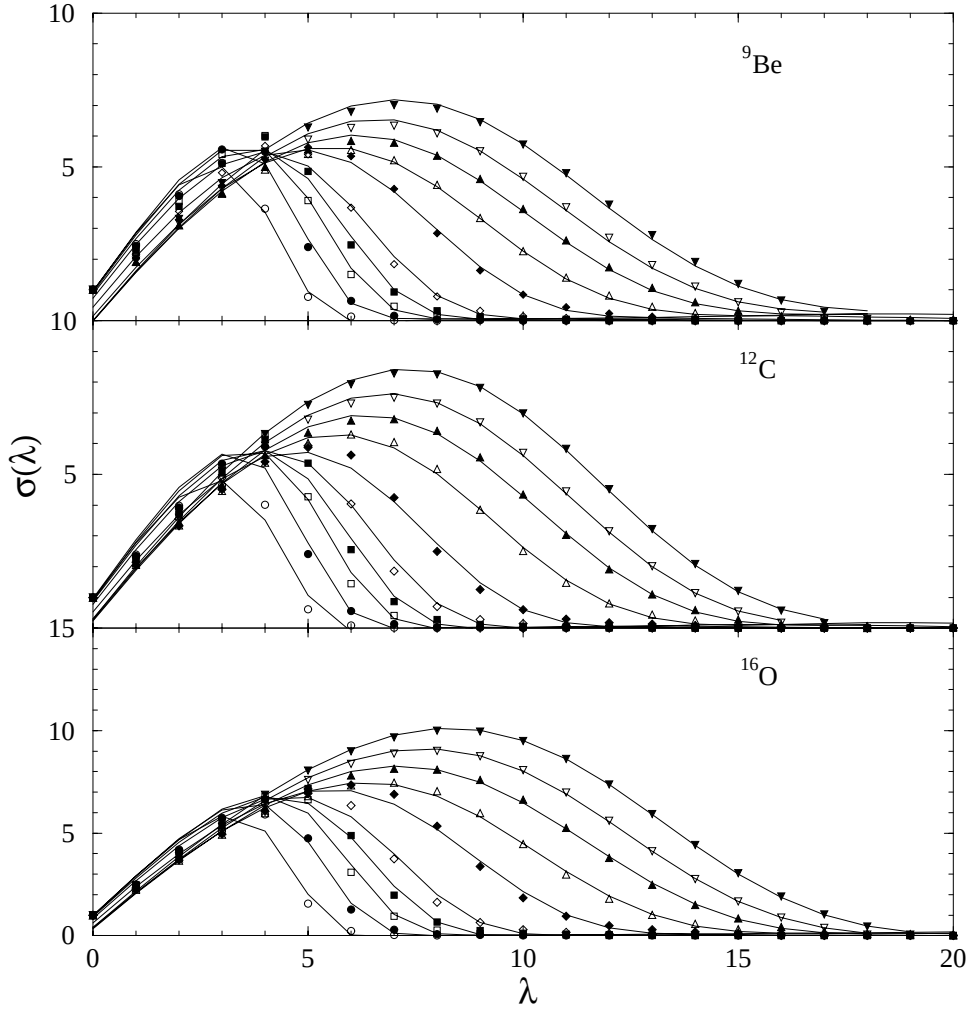

FIG. 1: The total partial reaction cross sections for proton scattering from ^{9}Be (top), ^{12}C (middle) and ^{16}O (bottom).

In Fig. 1, the partial reaction cross sections for proton scattering from ^{9}Be (top), ^{12}C (middle) and ^{16}O (bottom) obtained from the functional form calculations are compared with our data. Despite the foregoing comment, the calculated values are in excellent agreement with most of this data. It is clear that the shapes of these cross sections for proton scattering from light nuclei and for energies 65 MeV and below, differ somewhat from those at 100 MeV and above. Such differences persist with heavier targets. Also as the nuclear mass increases, the linear factor is more evident. The partial reaction cross sections for proton scattering from ^{19}F, ^{27}Al and ^{40}Ca obtained from the calculations using the simple functional form are compared with data in Fig. 2 in the top, middle and bottom panels respectively. That data are quite well reproduced. But as noted before, only a small number of values are of significance at 20 MeV. The predictions for the partial reaction cross sections for proton scattering from ^{63}Cu to higher mass nuclei are in excellent agreement with our data and such is evident in Figs. 3, 4 and 5. For these targets, the dominance of the linear term $(2l+1)$ of Eq. 3 in the fit to the low value partial wave data is evident for all energies including 20 MeV since now, even at that energy, a reasonable number of partial wave terms contribute

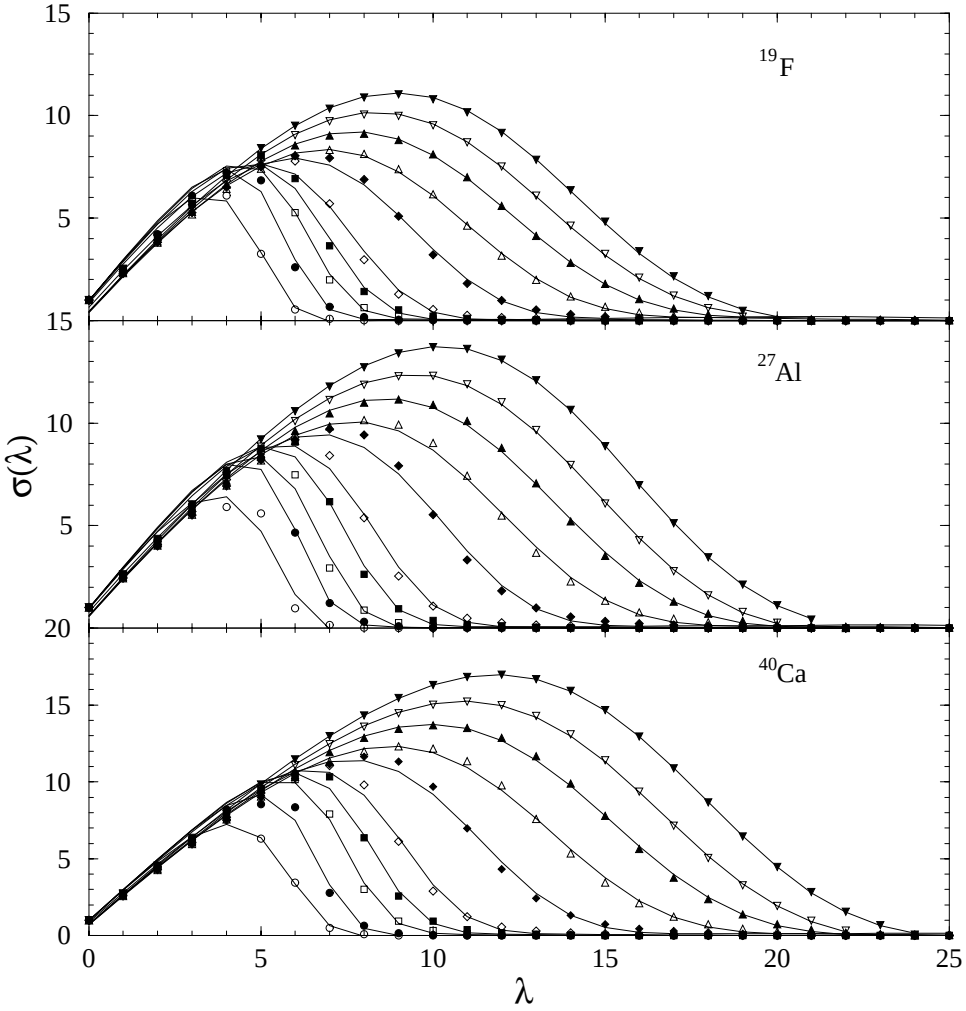

FIG. 2: Same as Fig. 1, but for ^{19}F (top), ^{27}Al (middle) and ^{40}Ca (bottom).

significantly to the reaction cross sections. Then l_0 is large enough so that the Wood-Saxon function in Eq. 3 essentially is constant for $0 \leq l \leq 5$ or more.

In Fig. 6 and 7, we plot the parameter values found for each specific energy. Therein, different symbols now indicate different nuclei. Empty circles represent the results for ^{9}Be, filled circles for ^{12}C, empty squares for ^{16}O, filled squares for ^{19}F, empty diamonds for ^{27}Al, filled diamonds for ^{40}Ca, empty up triangles for ^{63}Cu, filled up triangles for ^{90}Zr, empty left triangles for ^{118}Sn, filled left triangles for ^{140}Ce, empty down triangles for ^{159}Tb, filled down triangles for ^{181}Au, empty right triangles for ^{197}Au, filled right triangles for ^{208}Pb and the stars depict the values for ^{238}U. The l_0 parameter values are plotted as functions of $kA^{1/3}$ while the parameters a and ϵ are plotted as functions of k. It is clear that the parameters vary smoothly with energy. Of these, the linearity of l_0 with $kA^{1/3}$ is most evident and we find that

$$l_0(E, A) \sim kR + 2.3 \; ; \quad R \sim 1.32A^{\frac{1}{3}} \; , \tag{8}$$

is a best guess trend. Although, the variations of a and ϵ are not as smooth with k, overall they approximate roughly as linear variations with k. The respective trend lines are shown

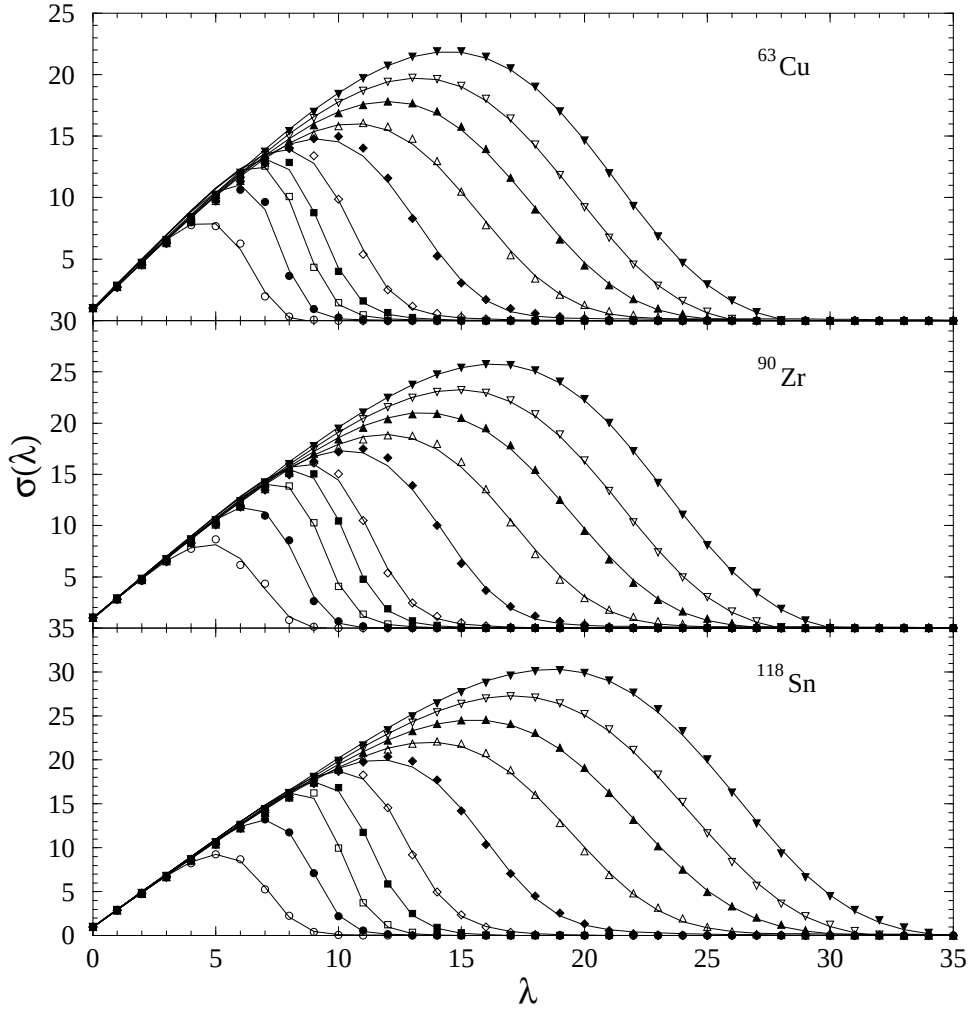

FIG. 3: Same as Fig. 1, but for ^{63}Cu (top), ^{90}Zr (middle) and ^{118}Sn (bottom).

in Fig. 7. From this, we find

$$a(E,A) \sim 1.02k - 0.25 \; ; \quad \epsilon \sim -1.5 \tag{9}$$

to be a simple mean value prescription that might be used in the integration formulas. However the spread of results about these means are significant. For best results then, one should consider each parameter set as points in an energy-mass tabulation and use a spline or similar interpolation to predict results for other energies, and perhaps, other nuclei. The best fit values of these parameters are available in tabular form [15].

The values of the total reaction cross sections determined using this simple functional form approximation are listed in Tables I and II as ratios to the actual values that were evaluated with the microscopic optical potentials, i.e. the data sums. In getting the results shown in the first table (R_I), the values of the three function parameters found from the fitting program (i.e. the tabulated parameter values [15]) were used to give the denominators. The results compare well to within a percent in most reflecting the quality of fit found by the search process. The ratios, R_{II}, that are listed in Table II, were found by using instead the integral results obtained using the three parameter sets defined by the average trend

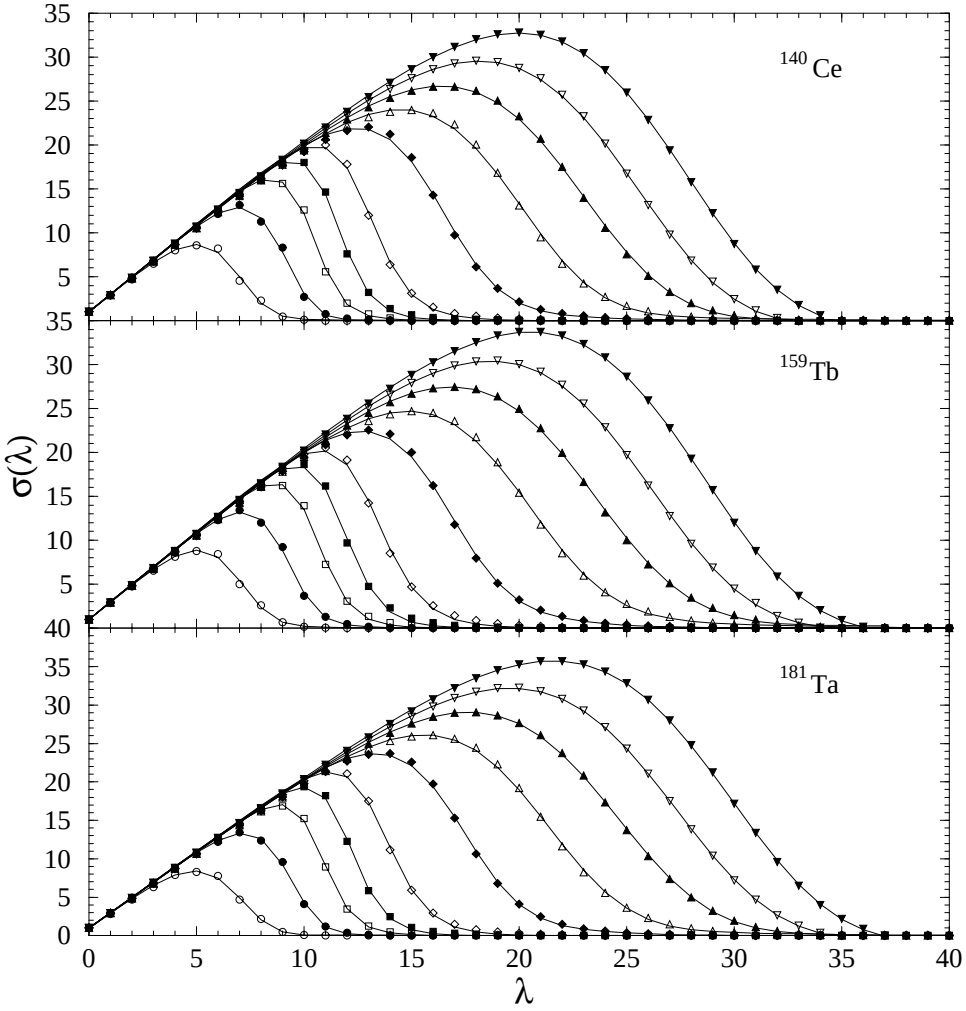

FIG. 4: Same as Fig. 1, but for ^{140}Ce (top), ^{159}Tb (middle) and ^{181}Ta (bottom).

function forms of Eqs. 8 and 9. In those calculations,

$$k = \frac{1}{\hbar c}\sqrt{E^2 - m^2c^4}, \tag{10}$$

was used in evaluating the denominators with the integral representation for the reaction cross sections. These ratios indicate that the integral approximation is good to 5% (ratios in the range 0.95 to 1.05) in some but not all cases. Notably at low energies (20 and 30 MeV) for all masses, and for almost all energies for ^{12}C, the reproductions are not good. Predominantly this was caused by the choice of linear forms for a and ϵ. If on the other hand, the tabled values of the parameters are used in the $n = 1$ formula of Eq. 7, the ratios again are one to within a few percent.

IV. CONCLUSIONS

The measured reaction cross sections for 20 to 300 MeV proton scattering from nuclei ranging in mass from ^{9}Be to ^{238}U are very well predicted by the calculations made using

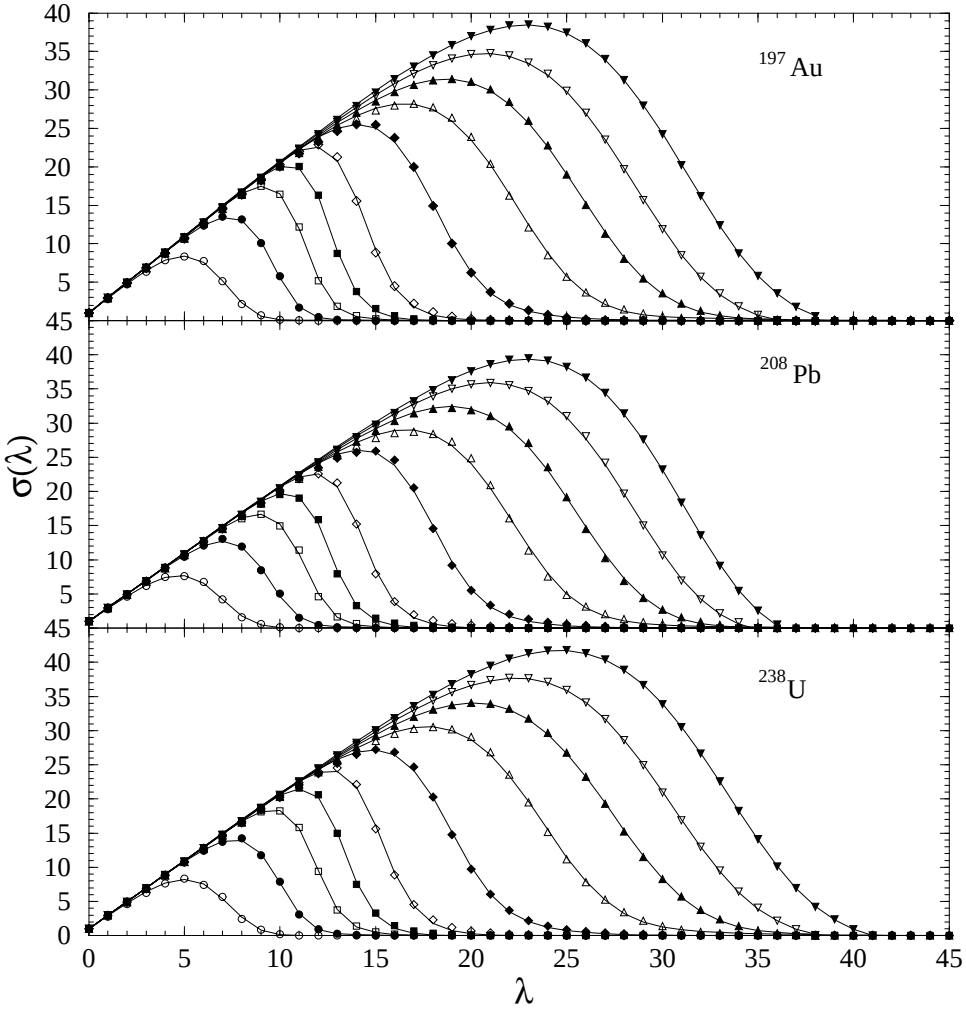

FIG. 5: Same as Fig. 1, but for ^{197}Au (top), ^{208}Pb (middle) and ^{238}U (bottom).

the g-folding model of the optical potential. Those calculated results gave a set of partial reaction cross sections in each case (for each angular momentum value of import) that vary smoothly with target mass and energy. Those variations are well reproduced by a simple 3 parameter function. The values of the parameters (l_0, a, ϵ) required to set those quality fits also are smooth functions of target mass and energy. We believe that such may be used as an interpolation tabulation with that simple functional sum to predict partial cross sections, and then by summation, the total reaction cross sections of proton-nucleus scattering. The extension of using an integral representation to specify the total reaction cross sections can be useful but also may diverge from measured values by 10% or more if a general linear (with k) behavior is adapted for the parameters a and ϵ.

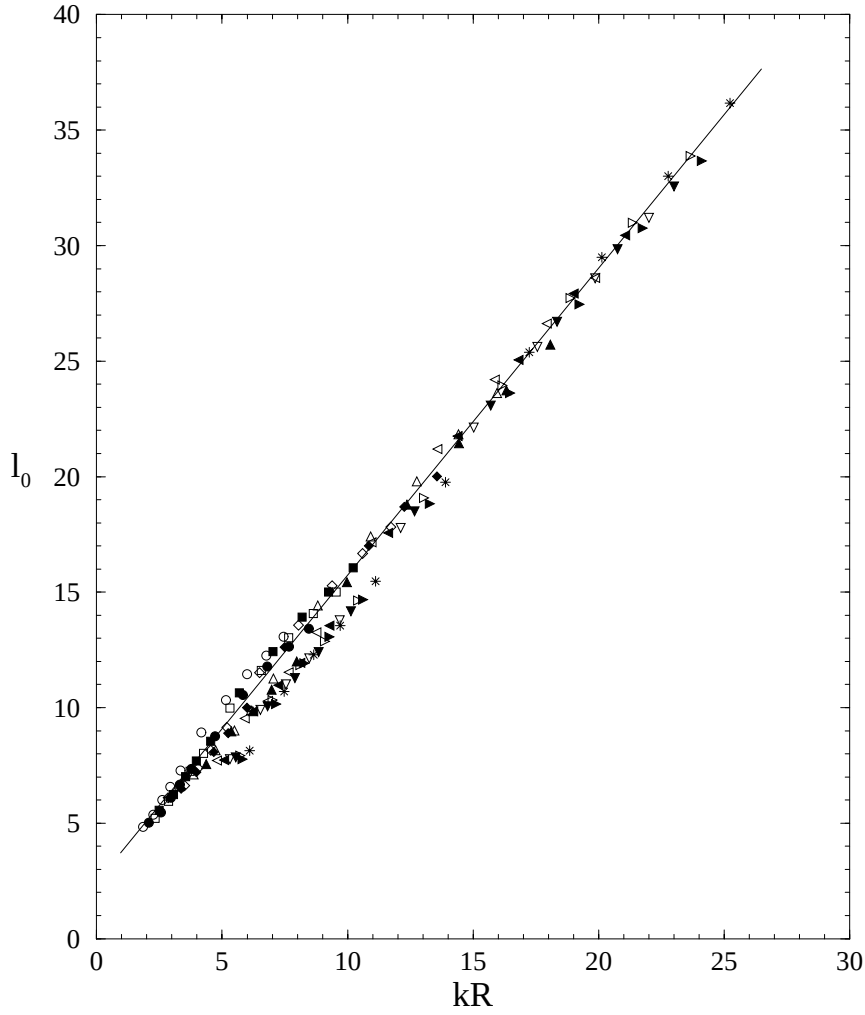

FIG. 6: The parameter l_0 of the simple functional form for the proton-nucleus partial reaction cross sections.

Acknowledgments

This research was supported by a research grant from the Australian Research Council.

---

[1] N. J. DiGiacomo, R. M. DeVries, and J. C. Peng, Phys. Rev. Lett. **45**, 527 (1980).

[2] C. R. Ramsey, L. W. Townsend, R. K. Tripathi, and F. A. Cucinotta, Phys. Rev. C **57**, 982 (1998).

[3] H. Geissel, G. Munzenberg, and K. Riisager, Annu. Rev. Nucl. Part. Sci. **45**, 163 (1995).

[4] J. P. Wefel, in *NATO ASI Series C: Mathematical and Physical Seiences*, edited by M. M. Shapiro and J. P. Wefel (Reidel, Dordrecht, Erice, Italy, 1987), vol. 220.

[5] J. W. Wilson et al., in *NATO ASI Series C: Mathematical and Physical Seiences*, edited by M. M. Shapiro (Reidel, Dordrecht, Erice, Italy, 1982), vol. 107.

[6] Y. Ikeda, J. Nucl. Sci. and Tech. (Japan) (2002), in press.

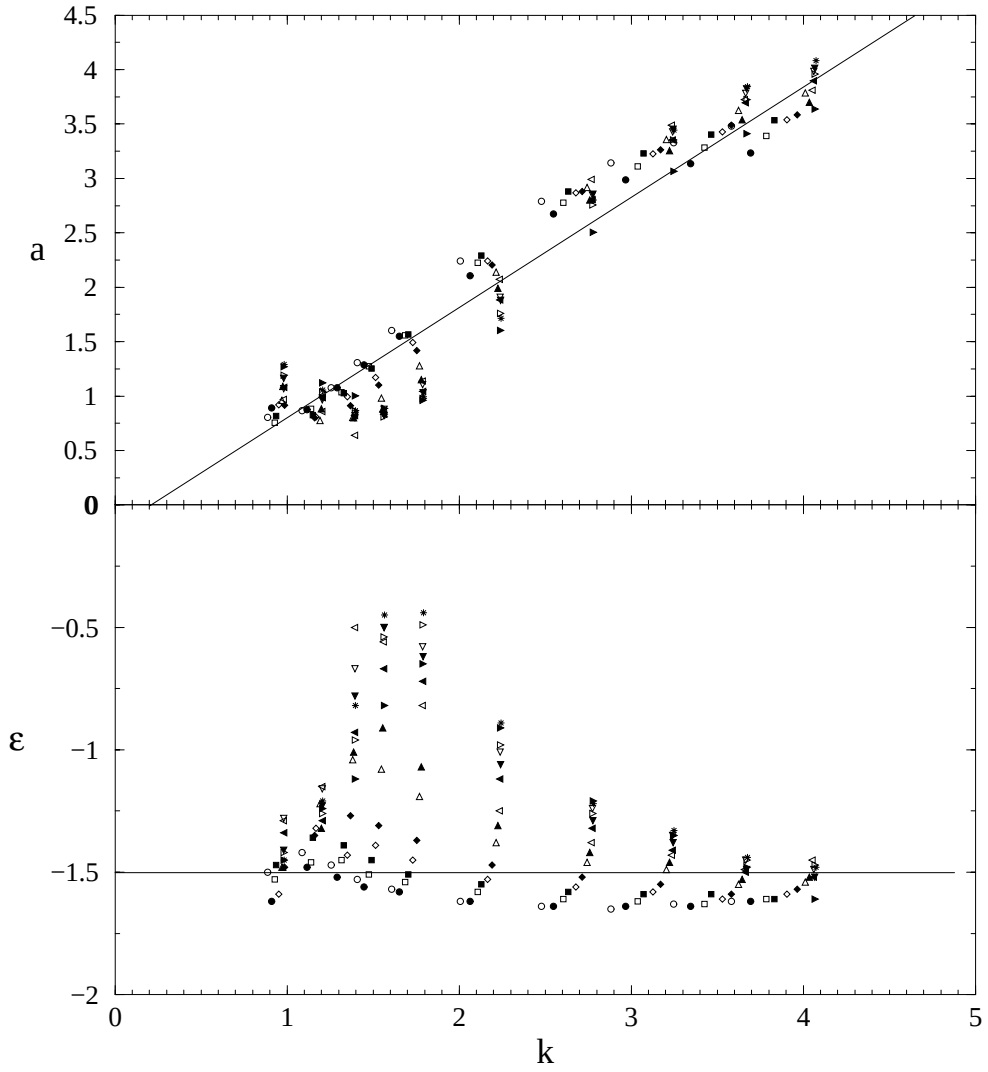

FIG. 7: Trend lines for the parameters a and ϵ of the simple functional form for the proton-nucleus partial reaction cross sections.

[7] W. Gudowski, K. Tucek, M. Ericsson, and J. Walleniu, J. Nucl. Sci. and Tech. (Japan) (2002), in press.

[8] F. Sheng, Y. Yanlin, Z. Zhixiang, Y. Hongwei, and L. Zhanglin, J. Nucl. Sci. and Tech. (Japan) (2002), in press.

[9] M. B. Chadwick, *Nuclear Data for Neutron and Proton Radiotherapy and for Radiation Protection*, vol. 63 of *ICRU Reports* (International Commission on Radiation Units and Measurements, Maryland, 2000).

[10] P. K. Deb, K. Amos, S. Karataglidis, M. B. Chadwick, and D. G. Madland, Phys. Rev. Lett. **86**, 3248 (2001).

[11] B. A. Brown, Phys. Rev. Lett. **85**, 5296 (2000).

[12] K. Amos, P. J. Dortmans, H. V. von Geramb, S. Karataglidis, and J. Raynal, Adv. in Nucl. Phys. **25**, 275 (2000).

[13] J. Raynal, *computer program dwba98* (1998).

TABLE I: Ratios of the total reaction cross sections formed as sums of the function defined partial cross sections and data.

Energy (MeV) =	20	30	40	50	65	100	150	200	250	300
^{9}Be	1.02	1.02	1.02	1.02	1.01	1.01	1.02	1.03	1.06	1.04
^{12}C	1.01	1.03	1.03	1.01	1.01	1.01	1.01	1.02	1.02	1.02
^{16}O	1.04	1.02	1.03	1.02	1.02	1.02	1.01	1.02	1.01	1.01
^{19}F	1.02	1.03	1.03	1.03	1.02	1.01	1.01	1.02	1.02	1.01
^{27}Al	1.01	1.03	1.04	1.03	1.02	1.01	1.01	1.01	1.01	1.00
^{40}Ca	1.01	1.03	1.03	1.03	1.02	1.02	1.01	1.01	1.00	1.00
^{63}Cu	1.01	1.02	1.02	1.03	1.03	1.02	1.02	1.01	1.01	1.00
^{90}Zr	1.00	1.01	1.01	1.02	1.02	1.02	1.01	1.01	1.00	1.00
^{118}Sn	1.00	1.00	1.01	1.01	1.02	1.01	1.01	1.00	1.00	1.00
^{140}Ce	1.00	1.00	1.01	1.00	1.01	1.01	1.01	1.00	1.00	1.00
^{159}Tb	1.00	1.00	1.00	1.00	1.00	1.01	1.01	1.01	1.00	1.00
^{181}Ta	1.00	1.00	1.00	1.00	1.00	1.01	1.01	1.00	1.00	1.00
^{197}Au	1.00	1.00	1.00	1.00	1.00	1.01	1.01	1.00	1.00	1.00
^{208}Pb	1.00	1.00	1.00	1.00	1.00	1.01	1.01	1.00	1.00	0.99
^{238}U	1.00	1.00	1.00	1.00	1.00	1.00	1.01	1.00	1.00	1.00

[14] S. Karataglidis, K. Amod, B. A. Brown, and P. K. Deb, Phys. Rev. C **65**, 044306 (2002).

[15] P. K. Deb and K. Amos, *Parameter values for a simple functional form for proton-nucleus total reaction cross sections* (2002), university of Melbourne preprint, UM-P-008/02.

TABLE II: Ratios of the total reaction cross sections formed using the (n=1) integral representation and data.

Energy (MeV) =	20	30	40	50	65	100	150	200	250	300
^{9}Be	1.06	0.95	0.93	0.94	0.96	0.94	1.00	1.02	1.05	1.01
^{12}C	1.24	1.10	1.08	1.09	1.10	1.15	1.11	1.11	1.12	1.10
^{16}O	1.16	1.04	1.02	1.02	1.04	1.00	1.05	1.07	1.07	1.05
^{19}F	1.09	0.98	0.95	0.95	0.98	0.96	1.01	1.02	1.03	1.04
^{27}Al	1.14	1.01	1.04	0.98	1.00	0.97	1.02	1.03	1.07	1.03
^{40}Ca	1.17	1.03	0.98	0.99	0.98	0.97	1.02	1.03	1.04	1.03
^{63}Cu	1.19	1.00	0.94	0.95	0.93	0.92	0.96	0.98	1.00	0.99
^{90}Zr	1.31	1.04	0.96	0.93	0.98	0.95	1.00	1.01	1.03	1.03
^{118}Sn	1.30	1.01	0.93	0.90	0.88	0.89	0.92	0.94	0.97	0.97
^{140}Ce	1.50	1.10	0.98	0.94	0.92	0.89	0.93	0.96	0.98	0.98
^{159}Tb	1.50	1.13	1.00	0.96	0.94	0.93	0.96	0.98	1.01	1.01
^{181}Ta	1.75	1.22	1.05	0.99	0.96	0.94	0.97	1.00	1.02	1.02
^{197}Au	1.64	1.22	1.05	0.97	0.94	0.91	0.93	0.95	0.97	0.97
^{208}Pb	2.04	1.32	1.11	1.02	0.98	0.94	0.96	0.98	1.00	1.03
^{238}U	2.00	1.26	1.06	0.98	0.93	0.93	0.93	0.95	0.97	0.98